Article

Research on the Spatiotemporal Evolution of Mangrove Forests in the Hainan Island from 1991 to 2021 Based on SVM and Res-UNet Algorithms

Chang Fu [1,2,3,†] (ID), Xiqiang Song [2,3,†], Yu Xie [3], Cai Wang [3], Jianbiao Luo [3], Ying Fang [3], Bing Cao [1] and Zixuan Qiu [1,2,3,*] (ID)

1   Hainan Yazhou Bay Seed Laboratory, Sanya Nanfan Research Institute, Hainan University, Sanya 572025, China
2   Key Laboratory of Genetics and Germplasm Innovation of Tropical Special Forest Trees and Ornamental Plants, Ministry of Education, College of Forestry, Hainan University, Haikou 570228, China
3   Intelligent Forestry Key Laboratory of Haikou City, College of Forestry, Hainan University, Haikou 570228, China
*   Correspondence: zixuanqiu@hainanu.edu.cn; Tel.: +86-156-0080-4604
†   These authors contributed equally to this work.

Abstract: Mangrove ecosystems play a dominant role in global, tropical, and subtropical coastal wetlands. Remote sensing plays a central role in mangrove conservation, as it is the preferred tool for monitoring changes in spatiotemporal distribution. To improve correlated estimation accuracies and explore the influencing mechanisms based on the mangrove ground survey, this study used a support vector machine (SVM) machine learning and Res-UNet deep learning algorithms to identify the land area of mangrove forests and the crown surface cover area of mangrove forests in the Hainan Island from 1991 to 2021. Both classification techniques were verified by a confusion matrix, which from 1991 to 2021, revealed overall accuracies of $93.11 \pm 1.54\%$ and $96.43 \pm 1.15\%$ for SVM and Res-UNet, respectively. Res-UNet was more accurate in identifying the crown surface cover area, whereas SVM was more suitable for obtaining the land area. Furthermore, based on the crown surface cover area of the mangrove forests on the Hainan Island, influencing mechanisms were analyzed through dynamic changes and landscape patterns. Since 1991, the Hainan Island mangrove forest area has increased, with the center of mass moving from coastal areas to the ocean and increasing the overall landscape fragmentation. Moreover, the change in the mangrove forests area was correlated with economic development and the increasingly urban population of the entire island. Altogether, the reliable assessment of the tropical mangrove forest land area and crown surface cover provides an important research foundation for the protection and restoration plans of tropical mangrove forests.

Keywords: mangrove forests; Hainan Island; deep learning; spatiotemporal evolution; influential mechanism

1. Introduction

Mangrove forests are an important type of coastal wetland that contain woody plant communities mainly distributed in the intertidal zones of tropical and subtropical regions [1]. These biomes constitute one of the most productive ecosystem types worldwide and maintain substantial social, ecological, and economic values for the natural environment and human society [2]. Specifically, mangrove forests play an important role in maintaining the ecological balance of coastlines and protecting the land from erosion [3]. Recently, these forests have also been recognized as the main contributor to "blue carbon sinks" in the global coastal zone, playing an important role in the suppression of ever-increasing atmospheric carbon dioxide concentrations [4]. Before the 21st century, mangrove forest areas were continuously reduced and degraded due to increasing socioeconomic threats, making them one of the most threatened ecosystems on the planet [5]. From 2000 to 2016, as

government departments turned their attention to greater protection, the damaging human activities against global mangrove forests gradually decreased; however, the number of mangrove forests lost because of natural factors increased during the same period [6]. To further protect and manage mangrove forests, it remains necessary to understand their spatiotemporal evolution, as well as their response and adaptation mechanisms to population growth, economic development, climate, and other factors [7]. Mangrove forests are usually located within a large area of inaccessible mudflats, which complicates any corresponding groundwork efforts [8]. Alternatively, the history of mapping the range of mangrove forests with remote sensing data dates to the 1970s [9]; advances in sensor technology have offered increasingly improved effective mapping and monitoring techniques.

Remote sensing has been widely used for the multi-scale and long-term monitoring of environments and natural resources [10]. Over the past three decades, optical and radar satellites commonly used in mangrove research have included Landsat, SPOT, IRS 1C, IRS 1D, ASTER, IKONOS, QuickBird, RADARSAT-1 SAR, ENVISAT ASAR, ERS-1 SAR, JERS-1, AIRSAR, and ALOS PALSAR. The first civilian Earth satellite, Landsat, was launched in 1972, and the first commercial satellite, SPOT, was launched in 1986 [11]. Optical satellites are used more frequently than radar satellites in mangrove studies. For example, Hauser et al. [12] studied the spatiotemporal dynamics of mangrove forests on the Ga Mau Peninsula, Vietnam, from 2004 to 2013 using SPOT satellite imagery; moreover, Proisy et al. [13] used IKONOS, QuickBird, and WorldView satellite images to map the evolution of mangrove forests within an abandoned aquaculture estuary area in India from 2001 to 2015. Landsat time series are often the most common satellite data used to monitor ecosystem change at larger scales [14]. For example, Gaw et al. [15] used Landsat remote sensing imagery to study the dynamics of mangrove forests in Tanintharyi, Myanmar, from 1989 to 2014. Hu et al. [16] showed that Landsat remote sensing image data are the most commonly used data for mangrove forest feature classification because: (1) Landsat imagery data of a 30 m medium resolution can effectively extract spatial information from mangrove forests; (2) it contains rich waveform information; (3) it requires relatively short time intervals for image acquisition; (4) it maintains a long history (>30 years); and (5) it is characterized by relatively low imaging costs. Therefore, Landsat imagery data were used in this study to ensure the spatiotemporal integrity of the mangrove forest data to the maximum extent possible.

Although remote sensing technology can provide continuous spatiotemporal data for monitoring ecosystem changes, the accuracy of information extraction is influenced by image classification techniques and sensor resolution [17]. In land cover classification studies, nascent shrubs and herbs remain difficult to classify due to their similar spectral properties [18]. Similarly, a separate study in China showed that agricultural lands, inland dwarf tree forests, shrub forests, and aquatic plants with highly similar spectral characteristics to mangrove forests were easily misclassified [19]. Abdi [20] found that the support vector machine (SVM) machine-learning algorithm produced the highest accuracy for distinguishing regenerating shrubs and herbaceous plants (overall accuracy, OA = 76%). Guo et al. [21] found that the U-Net deep learning algorithm obtained good classification results for mangrove forest identification by multilayer convolutional operations (OA = 81%); however, the image elements in a small area near the mangrove forests' boundary were also misclassified. In response to the degradation problem exposed by deep learning algorithms during network training, Li et al. [22] proposed a residual learning framework ResNet, which, in a classification study of tree species, achieved a classification accuracy of 90.9% for ResNet-18. Moreover, deep residual U-Net is also widely used in remote sensing image classification [23]. Cao and Zhang [24] proposed the Res-UNet network, which combines U-Net and Resnet, to extract multi-scale spatial features that can effectively improve the accuracy of tree species classification. Therefore, in this study, to address issues with mangrove forest misclassification in large-scale feature analyses, the SVM and Res-UNet algorithms were chosen to remotely monitor the mangrove forest distribution on Hainan Island and conduct a comparative analysis.

Remote sensing technology can also accurately explore the dynamic changes in small-scale mangrove reserves. For example, Ibharim et al. [25] used remote sensing techniques to monitor changes in the Matang Mangrove Reserve, Malaysia, between 1993 and 2011, proposing conservation recommendations in terms of species distributions and patch types. Similarly, Son et al. [26] studied changes in the Can Gio Biosphere mangrove reserve in Vietnam from 1989 to 2014 using Landsat imagery data, finding that ~24% of the mangrove forests in the reserve were converted to aquaculture farms during this period and providing suggestions to assist local managers with reserve development. Zhen et al. [27] used radar and optical satellites combined with an improved mangrove classification method to assess the spatial distribution and dynamics of mangrove forests in the Dongzhai Port Mangrove Reserve, China, to improve the development of conservation and management policies. Such small-scale mangrove reserve studies can provide more accurate data on species distribution and land type but are limited in their ability to capture the effects of climate, social benefits, and economic benefit changes. Therefore, exploring the large-scale spatiotemporal evolution of mangroves can provide ideas for upstream planning, an important component of their sustainable development. For example, Gilani et al. [28] used Landsat imagery to monitor changes in the mangrove cover and fragmentation in Pakistan to assess the conservation and sustainability of mangrove forests. Giri et al. [29] used similar techniques at two spatial resolutions to study the proportion, patterns, causes, and consequences of changes in mangrove cover in South Asia, which can regularly monitor and manage mangroves in this region. Considering the advantages and limitations of different research scopes, this study systematically explored the response and adaptation mechanisms between the spatiotemporal evolution of tropical mangrove forests, climate, and socioeconomic changes at the provincial/city/county levels hierarchically.

This study aimed to improve the accuracy of remote sensing estimates of tropical mangrove forest spatial distributions and to explore the influential mechanisms of the spatiotemporal evolution of tropical mangrove forests. Furthermore, this study aimed to achieve the following three research objectives: (1) compare the advantages and limitations of SVM machine-learning and Res-UNet deep learning algorithms for extracting spatial information from the mangrove forest; (2) explore the spatiotemporal evolution of tropical mangrove forests on the Hainan Island from 1991 to 2021; and (3) analyze the response and adaptation mechanisms between the spatiotemporal evolution of tropical mangrove forests and changes in climate, environment, and socioeconomic benefits.

2. Materials and Methods

2.1. Materials

2.1.1. Study Area

The Hainan Island is located at the southernmost tip of China, on the northern edge of the tropics, between $108°37'$ to $111°03'$ E and $18°10'$ to $20°10'$ N. The island covers an area of ~3.54×10^4 km^2, with a coastline of 1944.4 km, and maintains a tropical maritime monsoon climate. It has the richest mangrove species and the most extensive mangrove forest area in China, including 26 species of true mangrove plants and 12 species of semi-mangrove plants [29]. The mangrove forests of the Hainan Island are mainly distributed along the coastal areas of 12 cities and counties in the northeast, south, east, and west, including the cities of Haikou, Wenchang, Danzhou, and Sanya.

2.1.2. Ground Survey Data Sources

From January 2020 to September 2020, we organized over 200 people to identify the range of the mangrove forests and record the distribution of dominant tree species on the Hainan Island during the ground survey (Figure 1 and Table A1). In addition, during past ground surveys, other members of our team recorded site data for mangrove forests on the Hainan Island as follows: in 1991 (429 sites), in 1996 (423 sites), in 2000 (441 sites), in 2007 (510 sites), in 2010 (485 sites), in 2015 (508 sites); site data for other land types were: in 1991 (1747 sites), in 1996 (1777 sites), in 2000 (1814 sites), in 2007 (1816 sites),

in 2010 (1809 sites), in 2015 (1744 sites). Based on the range of the mangrove forests in the Hainan Island in 2020 and the site data previously surveyed by other members of the team, in October 2021, we conducted another ground survey and recorded data from 504 mangrove sites and 1805 other land-type sites. In addition, in each ground survey, all members of our team used a handheld GPS and Google Earth (Google Inc., Santa Clara County, CA, USA) to collect site data. The size of each site was 30 m × 30 m.
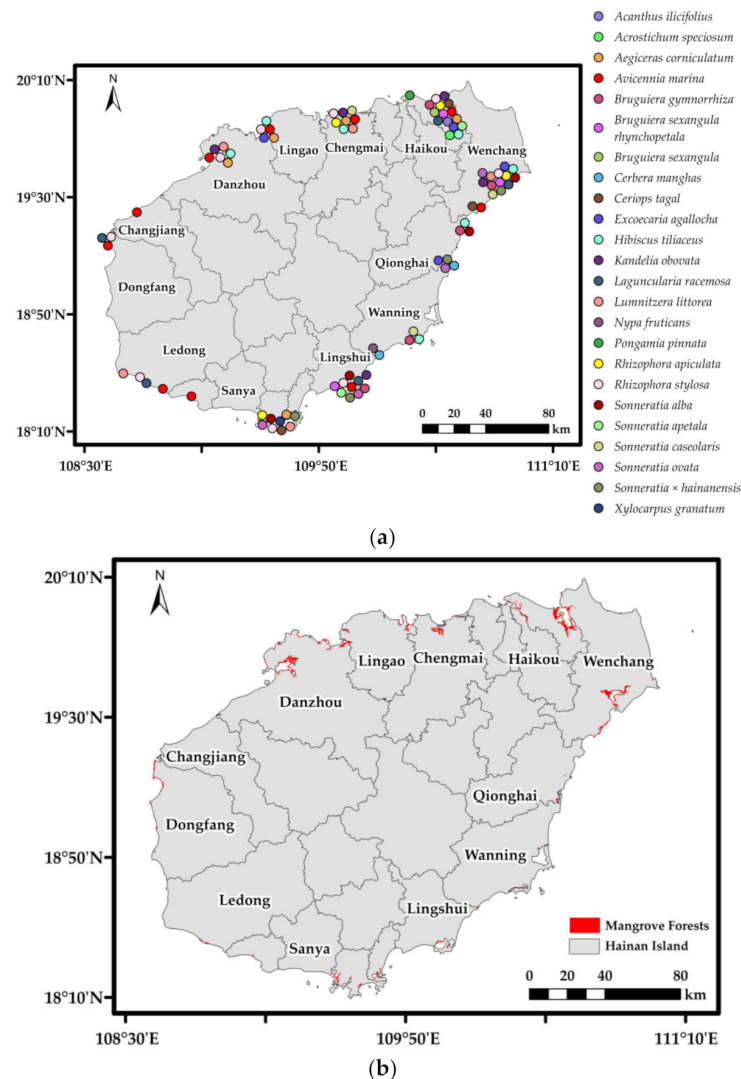
Figure 1. Ground survey data in 2020. (**a**) Distribution of dominant mangrove forest tree species in the Hainan Island. (**b**) Distribution range of mangrove forests in the Hainan Island.

2.1.3. Landsat Data Sources and Preprocessing

Landsat satellite image data were downloaded from the United States Geological Survey (USGS) for Earth Resources Observation and Science (https://www.usgs.gov/, accessed on 9 September 2022), from which the spatial resolution was 30 m. This study required images with a cloud coverage of less than 20%, and thus, compared and selected the Landsat satellite data obtained in 1991 (Landsat-5 TM), 1996 (Landsat-5 TM), 2000 (Landsat-5 TM), 2007 (Landsat-5 TM), 2010 (Landsat-5 TM), 2015 (Landsat-8 OLI), and 2021 (Landsat-8 OLI) (Table 1). Considering the large study area and complexity of the landscape, images of the same area were collected from adjacent years to reduce data loss related to cloudiness. The selected Landsat remote sensing image data were pre-processed with atmospheric correction, band combination, and image cropping. Because mangrove forests have more distinct spectral features in remote sensing image data,

especially a strong reflectance in the near-infrared (NIR) band, they are more easily classified than other land cover types [30]. To distinguish the mangrove forests, Landsat-5 TM usually uses B4 (NIR, 0.76–0.90 µm), B3 (Red, 0.63–0.69 µm), and B2 (Green, 0.52–0.60 µm) bands to synthesize standard false color feature images. In such standard false color feature images, mangrove forests typically appear as deep red. However, B5 (NIR, 0.85–0.89 µm), B4 (Red, 0.63–0.68 µm), and B3 (Green, 0.53–0.60 µm) bands were used from Landsat 8 OLI.

Table 1. Information about the Landsat data images used in the study.

Year	Landsat Data Acquisition Times					Satellite Sensor	Standard False Color
1991	15 June	20 August	30 October	30 October	16 April 1992		B4 (NIR, 0.76–0.90 µm),
1996	14 July	14 December	23 December	23 December	23 September 1995		B3 (Red, 0.63–0.69 µm),
2000	28 March	20 April	20 April	7 November	24 March 2001	Landsat-5 TM	B2 (Green, 0.52–0.60 µm)
2007	6 July	13 July	15 July	15 July	22 July		
2010	7 February	24 March	7 July	16 September	21 August 2009		
2015	16 April	16 April	5 September	17 November	8 March 2016	Landsat-8 OLI	B5 (NIR, 0.85–0.89 µm), B4 (Red, 0.63–0.68 µm),
2021	1 January	1 January	11 March	13 June	19 June		B3 (Green, 0.53–0.60 µm)

2.1.4. Population, Economy, and Climate Data Sources

This study was taken from the WorldClim data website (https://www.worldclim.org/data/index.html, accessed on 9 September 2022) where a spatial resolution of 2.5 m of monthly weather data over 1990–2018 years of history was downloaded. Then, the CNRM-CM6-1 model and the sustainable development scenario (SSP226) were selected in CMIP6 to download the monthly climate data with a spatial resolution of 2.5 m. The average minimum temperature (°C), average maximum temperature (°C), and total precipitation (mm) in 1991, 1996, 2000, 2007, 2010, 2015, and 2021 were sorted out in the TIFF format climate data set. Furthermore, the total population, urban population, rural population, GDP, and gross output fishery value were obtained from the Annual Statistical Report of Hainan Province in 1991, 1996, 2000, 2007, 2010, 2015, and 2021, respectively.

2.2. Methods

2.2.1. Support Vector Machine

The SVM machine-learning algorithm used here for supervised classification is based on the statistical learning theory and was originally developed to solve dichotomous classification problems [21]. SVM tries to identify the optimal thresholds that maximize the separation or bounds between the support vectors [31]. In another way, this requires finding the best hyperplane in a multidimensional space that splits two sets of vectors so that the vectors closest to the hyperplane (i.e., the support vectors) are as far away as possible from the hyperplane (Figure 2). Assuming that the Euclidean distance of the vector to the hyperplane is d_i, the minimum value of d_i is required to represent the shortest distance of this vector to the hyperplane. Accordingly, the mathematical expressions for the hyperplane $g(x)$ and d_i are defined by Equations (1) and (2):

$$g(x) = w^T \cdot x + b; \; w, \; x \in R^n \tag{1}$$

$$d_i = \frac{|g(x)|}{\|w\|} \tag{2}$$

where w and x are vectors in the n-dimensional space. x is a function variable and w is a normal vector. $\|w\|$ is the parametrization of the hyperplane.
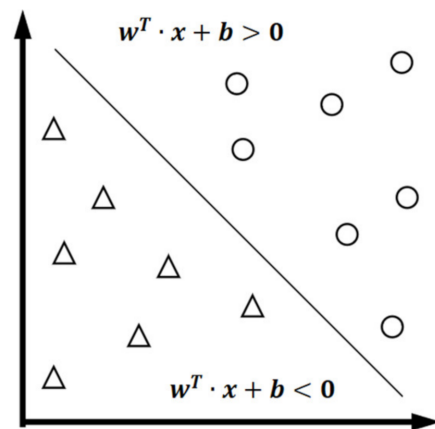
Figure 2. Visualization of the hyperplane separating the two types of vectors (assuming $g(x) = 0$).

In this study, the radial basis function (RBF) was selected as the kernel function, Gamma = 1, and the system default values were used for other parameters when SVM was used to establish the mangrove forests distribution model in the Hainan Island. The input band parameters were as follows: Landsat-5 TM: B4-Near IR (0.76–0.90 μm), B3-Red (0.63–0.69 μm), B2-Green (0.52–0.60 μm); Landsat-8 OLI: B5-Near IR (0.85–0.89 μm), B4-Red (0.63–0.68 μm), B3-Green (0.53–0.60 μm). The number of training samples selected for SVM machine-learning each year is as follows: in 1991 (312 mangrove sites and 1245 non-mangrove sites), in 1996 (304 mangrove sites and 1260 non-mangrove sites), in 2000 (318 mangrove sites and 1280 non-mangrove sites), in 2007 (380 mangrove sites and 1299 non-mangrove sites), in 2010 (351 mangrove sites and 1303 non-mangrove sites), in 2015 (374 mangrove sites and 1244 non-mangrove sites), and in 2021 (353 mangrove sites and 1296 non-mangrove sites). The size of a single sample is 30 × 30 m.

2.2.2. Res-UNet

U-Net was first applied to medical image segmentation [32]. Later, it was also widely used in remote sensing image classification [33]. The deep residual network ResNet can avoid the problem of gradient degradation in the process of network deepening [34]. This study used U-Net to equip the ResNet-18 backbone to train deep learning models (Figure 3) in order to increase the feature expression ability of the model [35]. Among them, ResNet-18 is a two-level ResNet residual unit, and the network structure of residual learning can be seen in Figure 4.

During model training, the average cross-entropy loss was used to calculate the model loss via the function presented in Equation (3):

$$loss = -\frac{1}{n} \sum_{i=1}^{n} y_i log a_i + (1 - y_i) log(1 - a_i) \tag{3}$$

where n represents the batch size; y_i and a_i are the predicted and true values of the ith sample in each batch, respectively. For the loss of the model, the network parameters were optimized using the Adam optimizer proposed by Kingma and Ba [36], according to Equation (4):

$$\theta_t = \theta_{t-1} - \alpha * \hat{m}_t / \left(\sqrt{\hat{v}_t} + \varepsilon \right) \tag{4}$$

where t is the number of training iterations, α is the learning rate, m is the exponential moving average of the gradient, and v is the exponential moving average of the gradient squared. The "ε" is usually a constant with a value of 1×10^{-8}.
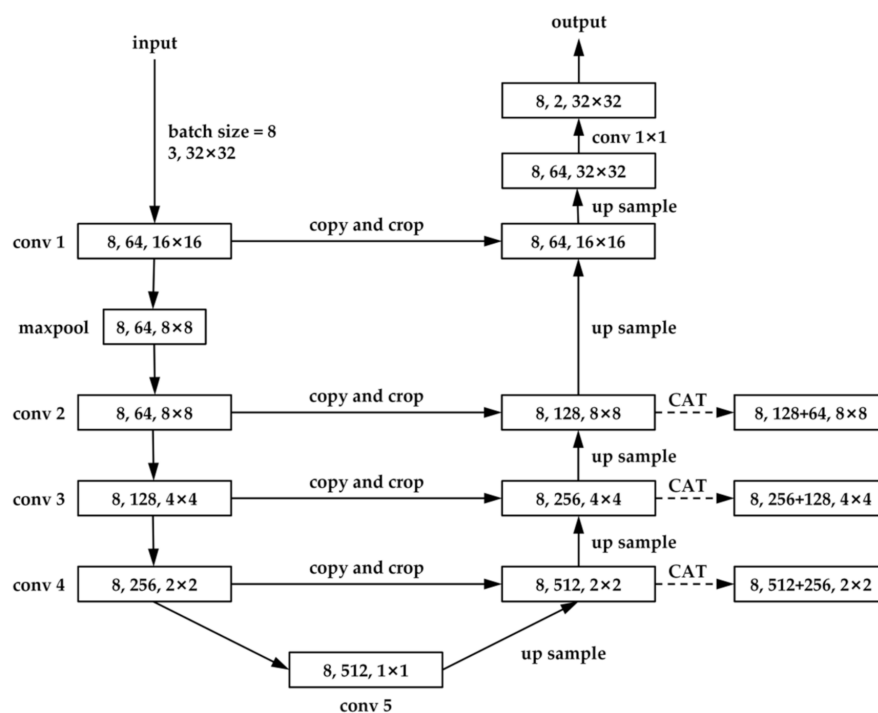
Figure 3. Network structure of Res-UNet. "conv" referring to the feature map. "CAT" is a method of concatenating feature maps with different numbers of channels.
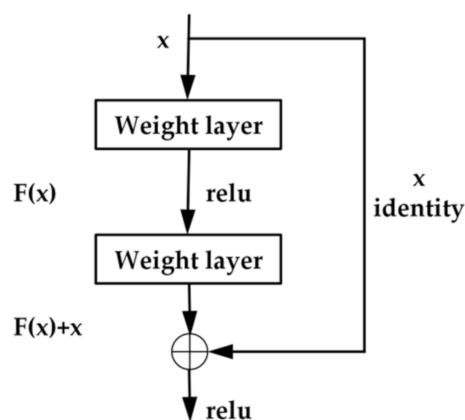
Figure 4. Network structure of residual learning. "F(x)" refers to the residual and "x" is the feature mapping of the output of the previous layer ResNet.

This study used Python based on the TensorFlow deep learning framework. The hardware configuration of this operating platform included a Lenovo ThinkStation P620 AMD3955WX 64G and an NVIDIA Quadro RTX4000 8G GPU. Based on the site data from the ground survey and the distribution range of mangrove forests from the ground survey in 2020, the distribution range of mangrove forests in the Haikou, Wenchang, and Danzhou cities were mapped by visual interpretation in Landsat remote sensing images. When Res-UNet trained the model of mangrove forest distribution on the Hainan Island, the Landsat remote sensing images were cut, referring to the visually interpreted mangrove distribution range. The slice size was set to 32×32 pixels, the batch size = 8, the backbone model was set to ResNet–18, and the default values for other parameters were used. The input band parameters were as follows: Landsat-5 TM: B4-Near IR (0.76–0.90 μm), B3-Red (0.63–0.69 μm), and B2-Green (0.52–0.60 μm); Landsat-8 OLI: B5-Near IR (0.85–0.89 μm), B4-Red (0.63–0.68 μm), and B3-Green (0.53–0.60 μm). Finally, the training samples for Res-UNet deep learning were obtained as follows: in 1991 (780 sites), in

1996 (873 sites), in 2000 (767 sites), in 2007 (875 sites), in 2010 (928 sites), in 2015 (1050 sites), and in 2021 (1201 sites). The size of a single sample is 32 × 32 pixels.

2.2.3. Accuracy Assessment

Here, two metrics, the Kappa coefficient, and the OA were used to evaluate the classification accuracy of SVM and Res-UNet, respectively. Both metrics were calculated based on a confusion matrix, which provided a clear picture of the number of features correctly and incorrectly classified [37]. Specifically, the Kappa coefficient is typically used to test the consistency of results and measure the effectiveness of classifications, whereas OA is the ratio of correctly classified categories to the total category number [21]. Of the sites obtained each year, approximately 30% were selected as a validation sample. The sample types were divided into mangrove and non-mangrove (other land types). The number of validation samples selected each year is as follows: in 1991 (117 mangrove sites and 502 non-mangrove sites), in 1996 (119 mangrove sites and 517 non-mangrove sites), in 2000 (123 mangrove sites and 534 non-mangrove sites), in 2007 (130 mangrove sites and 517 non-mangrove sites), in 2010 (134 mangrove sites and 506 non-mangrove sites), in 2015 (134 mangrove sites and 500 non-mangrove sites), and in 2021 (151 mangrove sites and 509 non-mangrove sites). the size of a single sample is 30 × 30 m. The confusion matrix was used to evaluate the classification results of the model, and the precise equations for *OA* and *Kappa*, are presented in Equations (5) and (6):

$$OA = \frac{\sum_{i=1}^{2} a_{ii}}{N} \tag{5}$$

$$Kappa = \frac{OA - \frac{\sum_{i=1}^{2} a_{i+} * a_{+i}}{N^2}}{1 - OA}, a_{i+} = \sum_i a_{ij}, a_{+i} = \sum_j a_{ij} \tag{6}$$

where a_{ii} denotes the accurate values of i predicted to be i, a_{ij} denotes the values of i predicted to be j, and N is the total number of samples.

2.2.4. Dynamic Change and Landscape Pattern Analysis

Here, the area of mangrove forest cover change was evaluated and compared based on the mangrove distribution of 1991, 1996, 2000, 2007, 2010, 2015, and 2021. The annual rate of change in the crown surface area was used to analyze the mangrove forest changes over the last 30 years for six stages: 1991–1996, 1996–2000, 2000–2007, 2007–2010, 2010–2015, and 2015–2021. Specifically, the annual rate of change in the crown surface area was calculated using the formula proposed by Puyravaud [38]:

$$r = \frac{1}{t_2 - t_1} ln \frac{A_2}{A_1} \tag{7}$$

where r is the annual percentage change rate; t_1 and t_2 are the starting and ending years at the time of calculation, respectively; and A_1 and A_2 are the corresponding areas in t_1 and t_2, respectively.

In evaluating the spatiotemporal changes in the landscape patterns of mangrove forests, landscape indices, such as shape complexity and patch fragmentation, can further reveal the impacts of human activities [39]. Five landscape indices were selected based on the actual situation of the study area: the number of patches (NP), patch density (PD), maximum patch index (LPI), landscape shape index (LSI) and aggregation index (AI), where NP reflects the spatial pattern of the landscape; PD describes the degree of landscape fragmentation; LPI indicates the expansion or fragmentation of the largest mangrove forest patches, reflecting the health of the mangrove forests in the core area; LSI determines the shape changes of the patch, corresponding to the resistance abilities of the mangrove forests to external disturbances; and AI reflects the connectivity and degree of aggregation and

dispersion within mangrove forest patches [40]. PD, LSI, and AI were calculated according to Equations (8)–(10) [39]:

$$PD = \frac{NP}{A}, \; PD > 0 \tag{8}$$

$$LSI = \frac{0.25E}{\sqrt{A}}, \; LSI \geq 1 \tag{9}$$

$$AI = \frac{p_{ij}}{max \; p_{ij}} \times 100 \tag{10}$$

where A is the total landscape area (ha), E is the total length of the edge in the landscape, and p_{ij} represents the number of adjacent patches in patches of the same type as the landscape, i represents a landscape type, and j represents patches of the same type as i.

The mangrove mass center offset trajectory can reflect the spatial distribution of mangrove forests over different years, an important factor when studying the dynamic changes over certain periods of time. Here, the principle was to adopt the change in the mass center coordinates of the landscape patches to reflect the change laws of the mangrove area mass center distributions. The center of mass formula was derived from Li et al. [41] (Equation (11)):

$$X_t = \frac{\sum_{i=1}^{N}(C_{ti}X_i)}{\sum_{i=1}^{N} C_{ti}}, \; Y_t = \frac{\sum_{i=1}^{N}(C_{ti}Y_i)}{\sum_{i=1}^{N} C_{ti}} \tag{11}$$

where X_t and Y_t denote the latitude and longitude coordinates of the landscape mass center in year t, respectively; X_i and Y_i are the latitude and longitude coordinates of the mass center of the ith patch of a landscape, respectively; C_{ti} is the area of the ith patch, and N is the total number of landscape patches.

2.2.5. Statistical Analysis of Driving Forces

Zheng and Takeuchi [42] showed that mangroves vary over space and time, with changes related to the climate, environment, and socioeconomic benefits. To quantify the main drivers affecting the evolution of mangrove landscapes, this study conducted a Pearson bivariate correlation analysis of the mangrove area with socioeconomic and natural environmental indicators. Eight indicators were selected for the study area: total population, urban population, rural population, GDP, gross production fishery value, average annual rainfall, minimum temperature, and maximum temperature.

3. Results

3.1. Analysis of the Classification Results

3.1.1. Classification Results of SVM Machine Learning

The SVM classification results are shown in Figure A1 in Appendix A. Confusion matrix calculations were used to summarize the producer accuracy (PA), user accuracy (UA), OA metrics, and Kappa coefficients. The SVM classification accuracy was the highest in 1996 and 2021 (Table 2), with the OA and Kappa coefficients at >94% and >0.80, respectively. The lowest classification accuracy was recorded in 2010 (OA and Kappa coefficients of 91.6% and 0.71, respectively). The primary classification task was to identify the mangrove forest presence; however, the spectral information of other land types can influence the classification results. The highest PA of the mangrove forests was recorded in 1996 (77.3%), and although the overall classification results of SVM were high, the identification results of the mangrove forests remained relatively inaccurate as the probability of the mangrove forests being misclassified persisted.

Table 2. Accuracy assessment of SVM classification results from mangrove forests in the Hainan Island during 1991–2021, where μ depicts the average values.

Period	Classified	Ground-Truth			Summary	
		Mangrove	**Non-Mangrove**	**Total**	**PA**	**UA**
1991	Mangrove	79	7	86	67.5%	91.9%
	Non-Mangrove	38	495	533	98.6%	92.9%
	Total	117	502	619	83.1μ	92.4μ
					OA = 92.7%	Kappa = 0.74
1996	Mangrove	92	7	99	77.3%	92.9%
	Non-Mangrove	27	510	537	98.7%	95.0%
	Total	119	517	636	88.0μ	94.0μ
					OA = 94.65%	Kappa = 0.81
2000	Mangrove	79	2	81	64.2%	97.5%
	Non-Mangrove	44	532	576	99.6%	92.4%
	Total	123	534	657	81.9μ	95.0μ
					OA = 93.00%	Kappa = 0.74
2007	Mangrove	80	2	82	61.5%	97.6%
	Non-Mangrove	50	515	565	99.6%	91.2%
	Total	130	517	647	80.6μ	94.4μ
					OA = 92.0%	Kappa = 0.71
2010	Mangrove	83	3	86	61.9%	96.5%
	Non-Mangrove	51	503	554	99.4%	90.8%
	Total	134	506	640	80.7μ	93.7μ
					OA = 91.6%	Kappa = 0.71
2015	Mangrove	96	2	98	71.6%	98.0%
	Non-Mangrove	38	498	536	99.6%	92.9%
	Total	134	500	634	85.6μ	95.4μ
					OA = 93.7%	Kappa = 0.79
2021	Mangrove	114	1	115	75.5%	99.1%
	Non-Mangrove	37	508	545	99.8%	93.2%
	Total	151	509	660	87.7μ	96.2μ
					OA = 94.2%	Kappa = 0.82

3.1.2. Classification Results of Res-UNet Deep Learning

The classification results of the Res-UNet deep learning algorithm are shown in Figure A2 in Appendix A. The extracted sample labels were divided into two categories: mangrove and non-mangrove forests. The confusion matrix was selected for accuracy verification, besides the PA, UA, OA, and Kappa coefficient calculations, for the classification results of the mangrove forests. When comparing the validation results across different years (Table 3), it was found that Res-UNet produced superior classification results (OA, 95%; Kappa coefficients, >0.80). Among them, the best classification accuracy was achieved in 2021 (OA and Kappa coefficient of 97.6% and 0.93, respectively), and the worst classification accuracy appeared in 1996 (OA and Kappa coefficient values of 95.3% and 0.83, respectively). Few mangrove forests were misclassified (low errors) using this deep learning algorithm (Table 3), resulting in high PA values in all the mangrove forest classes (reaching a maximum of 93.4% in 2021).

Table 3. Accuracy assessment of Res-UNet classification results of mangrove forests in the Hainan Island during 1991–2021, where µ depicts the averaged values.

Period	Classified	Ground-Truth			Summary	
		Mangrove	**Non-Mangrove**	**Total**	**PA**	**UA**
1991	Mangrove	92	3	95	78.6%	96.8%
	Non-Mangrove	25	499	524	99.4%	95.2%
	Total	117	502	619	89.0µ	96.0µ
					OA = 95.5%	Kappa = 0.84
1996	Mangrove	93	4	97	78.2%	95.9%
	Non-Mangrove	26	513	539	99.2%	95.2%
	Total	119	517	636	88.7µ	95.5µ
					OA = 95.3%	Kappa = 0.83
2000	Mangrove	106	4	110	86.2%	96.4%
	Non-Mangrove	17	530	547	99.3%	96.9%
	Total	123	534	657	92.7µ	96.6µ
					OA = 96.8%	Kappa = 0.89
2007	Mangrove	108	1	109	83.1%	99.1%
	Non-Mangrove	22	516	538	99.8%	95.9%
	Total	130	517	647	91.4µ	97.5µ
					OA = 96.5%	Kappa = 0.88
2010	Mangrove	115	3	118	85.8%	97.5%
	Non-Mangrove	19	503	522	99.4%	96.4%
	Total	134	506	640	92.6µ	96.9µ
					OA = 96.6%	Kappa = 0.89
2015	Mangrove	112	1	113	83.6%	99.1%
	Non-Mangrove	22	499	521	99.8%	95.8%
	Total	134	500	634	91.7µ	97.5µ
					OA = 96.4%	Kappa = 0.88
2021	Mangrove	141	6	147	93.4%	95.9%
	Non-Mangrove	10	503	513	98.8%	98.1%
	Total	151	509	660	96.1µ	97.0µ
					OA = 97.6%	Kappa = 0.93

The cross-entropy loss curve of the Res-UNet model is shown in Figure 5. Under the optimal model, the batch size was eight. After ~5000 training iterations, the loss of Res-UNet stabilized at 0.1, where the model weights gained certainty.
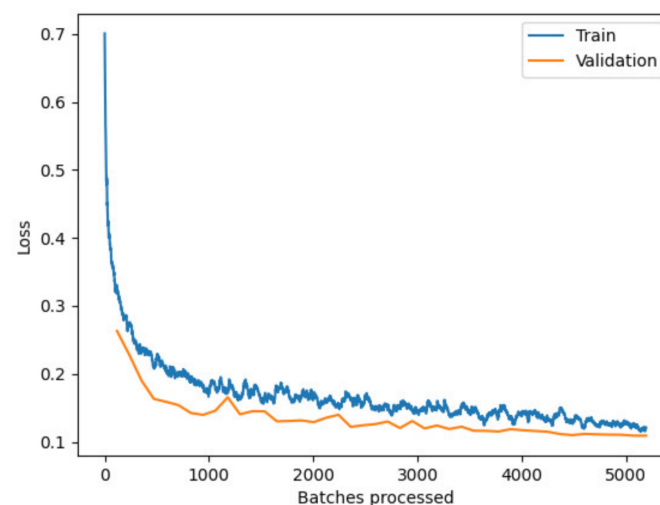
Figure 5. Res-UNet loss curve, where the *x*-axis indicates the number of training iterations.

3.1.3. Comparison of Mapping Results between SVM Machine Learning and Res-UNet Deep Learning

The SVM and Res-UNet classification results were compared with ground truth remote sensing imagery data to analyze the ability of the two algorithms to identify the distribution range of mangrove forests on the Hainan Island (Figure 6). Here, it was found that Res-UNet was more accurate in identifying the crown surface cover area, whereas SVM better reproduced the land area covered by entire wetlands or protected areas, including mangrove forests. The inability of SVM to distinguish mangrove forests from water and aquatic plants was evident (Figure 6a,b); therefore, the extracted mangrove distributions were more contiguous. Furthermore, numerous pixels with mixed low trees and shrubs were misclassified as "mangrove forests" (Figure 6e,f). In Figure 6c,d, an under-classification is observed due to the non-recognition of mangrove forests. In contrast, Res-UNet more accurately distinguished mangrove forests from other feature types with similar spectral information within mixed vegetation areas, greatly reducing the probability of mangrove forest misclassification on a large scale.
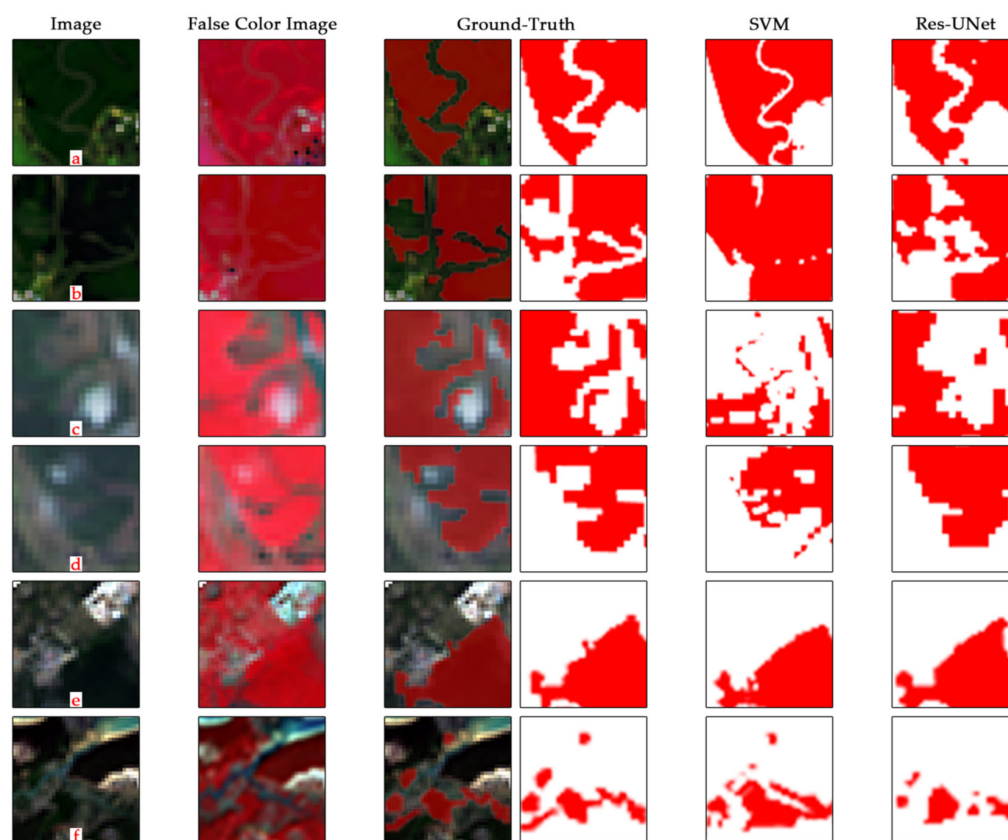
Figure 6. Illustrative examples of the classification method limitations for SVM and Res-UNet: (**a**,**b**) Haikou City, (**c**,**d**) Wenchang City, (**e**,**f**) Danzhou City; red represents mangrove forests, and white represents all other land types, each square is captured from a 30 m Landsat remote sensing image, and the side length is about 975 × 975 m.

3.2. Analysis of Spatiotemporal Changes of Mangrove Forests in the Hainan Island

3.2.1. Change in Mangrove Forest Crown Surface Cover Area during 1991–2021

Based on the validation of the Res-UNet algorithm, this trained model was applied to a large-scale mangrove forest crown surface mapping to compare the extent of the mangrove forest crown coverage changes in 1991, 1996, 2000, 2007, 2010, 2015, and 2021 on the Hainan Island. The crown surface cover area of the total mangrove forests on the Hainan Island in each of these seven periods was 1740.15, 2076.66, 1984.68, 2371.59, 2694.78, 2233.80, and 3438.63 ha, respectively (Figure 7 and Table 4). The mangrove forests

were mainly distributed over 12 cities and counties around the coast of the Hainan Island. By 2021, the forest crown surface cover areas in the cities of Haikou, Wenchang, and Danzhou increased, whereas those of the Wanning City, Ledong Li Autonomous County, and Changjiang Li Autonomous County receded during the analysis period. In addition, Wanning City, Ledong Li Autonomous County, Lingshui Li Autonomous County, and Changjiang Li Autonomous County were characterized by the disappearance of mangrove forests in individual years, with mangrove forests in Changjiang Li Autonomous County only present in 2000 and 2010. Overall, the mangrove forest crown surface cover area in the Hainan Island showed an increasing trend over the last three decades, with a net increase of 1698.48 ha from 1991 to 2021, representing an annual change rate of 2.27% (Table 4). The highest growth rate of the surface cover area of the mangrove forest crown was recorded throughout the analysis period in Dongfang City (16.24%), whereas the annual change rate peaked in the autonomous Ledong Li County from 2007 to 2021 ($\leq$35.50%).
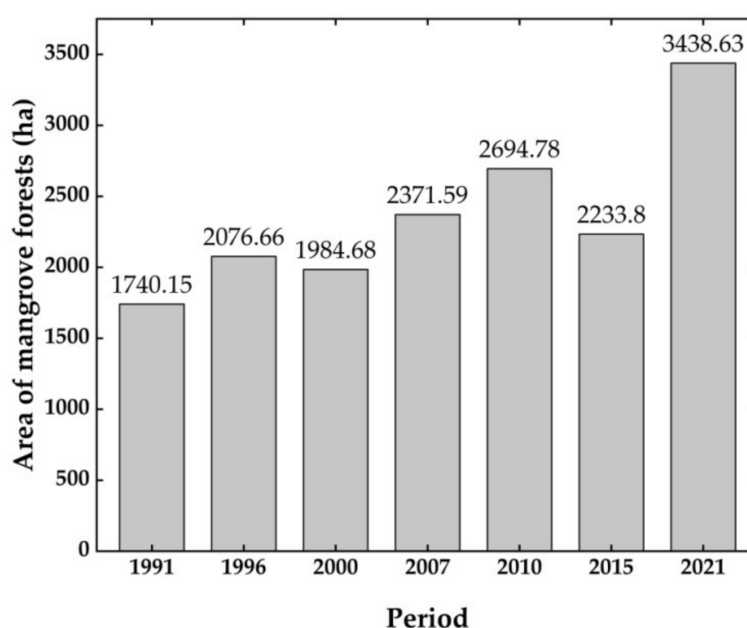
Figure 7. Trends of mangrove forest crown cover area in the Hainan Island during 1991–2021.

Table 4. Mangrove forest crown surface cover area (ha) and annual rate of area change (%) in the Hainan Island and in each city/county for every year of analysis.

City/County	Mangrove Forests Crown Cover (ha)							Annual Rate of Change (%)
	1991	1996	2000	2007	2010	2015	2021	
Haikou	898.20	1259.73	1221.12	1343.07	1294.74	1233.09	1183.59	0.92
Sanya	49.50	14.76	3.06	4.95	35.91	13.14	57.96	0.53
Wenchang	286.83	552.24	356.94	598.95	755.19	449.82	1083.42	4.43
Qionghai	25.02	1.26	11.61	6.12	41.31	1.80	32.13	0.83
Wanning	4.95	0.00	2.43	0.90	0.00	0.00	6.3	0.80
Chengmai	48.06	63.45	53.01	36.54	66.78	98.82	191.97	4.62
Lingao	46.71	9.9	24.39	42.3	80.01	40.23	129.96	3.41
Danzhou	377.73	155.07	277.29	319.86	369.18	364.86	610.56	1.60
Dongfang	0.63	18.54	33.84	16.29	9.36	30.51	82.17	16.24
Ledong	0.00	0.00	0.00	0.09	3.51	0.36	12.96	35.50 *
Lingshui	2.61	0.00	0.27	2.52	38.07	1.17	47.61	9.68
Changjiang	0.00	0.00	0.72	0.00	0.72	0.00	0.00	0.00 *
Total Area	1740.15	2076.66	1984.68	2371.59	2694.78	2233.80	3438.63	2.27

* Monitoring time starts from the year that mangrove forests appeared.

The changes in the surface cover area of the mangrove forest crown were compared and analyzed for each city and county in the Hainan Island across six periods: 1991–1996, 1996–2000, 2000–2007, 2007–2010, 2010–2015, and 2015–2021. Although the surface cover

area increased for all cities and counties in the Hainan Island over the analysis period (Table 4), the observed growth was unstable in terms of phase changes. The surface cover area decreased in the Hainan Island from 1996 to 2000 and 2010 to 2015 (annual rates of change: -1.13% and -3.75%, respectively; Table 5), while the highest growth rate in the island was observed from 2015 to 2021 ($7.19\% \cdot yr^{-1}$). However, the area of surface coverage of the mangrove forest crown in Haikou City decreased in the three phases from 2007 to 2021. Conversely, the crown surface cover area increased in Chengmai County from 2007 to 2021. In addition, the mangrove forest crown surface cover area in Lingao County and Danzhou City increased between 1996 and 2010, and the crown surface coverage of Lingshui Li Autonomous County also showed an increasing trend from 2000 to 2010.

Table 5. Annual rate of change (%) in the crown surface cover area of mangrove forests in the Hainan Island during 1991–1996, 1996–2000, 2000–2007, 2007–2010, 2010–2015, and 2015–2021.

City/County	Annual Rate of Change					
	1991–1996	1996–2000	2000–2007	2007–2010	2010–2015	2015–2021
Haikou	6.77	−0.78	1.36	−1.22	−0.98	−0.68
Sanya	−24.20	−39.34	6.87	66.05	−20.11	24.73
Wenchang	13.10	−10.91	7.39	7.73	−10.36	14.65
Qionghai	−59.77	55.52	−9.15	63.65	−62.67	48.03
Wanning	0.00	0.00	−14.19	0.00	0.00	0.00
Chengmai	5.56	−4.49	−5.32	20.10	7.84	11.07
Lingao	−31.03	22.54	7.87	21.25	−13.75	19.54
Danzhou	−17.81	14.53	2.04	4.78	−0.24	8.58
Dongfang	67.64	15.04	−10.44	−18.47	23.63	16.51
Ledong	0.00	0.00	0.00	122.12	−45.55	59.73
Lingshui	0.00	0.00	31.91	90.51	−69.65	61.77
Changjiang	0.00	0.00	0.00	0.00	0.00	0.00
Hainan Island	3.54	−1.13	2.54	4.26	−3.75	7.19

3.2.2. Spatial Distribution and Changes in Mangrove Forests during 1991–2021

The landscape-level pattern index can reflect the corresponding change characteristics of the entire study area (Figure 8). From 1991 to 2021, the NP, PD, and LSI of mangrove forests in the Hainan Island showed repeated trends of decreasing, followed by an increase. NP and LSI both reached a maximum in 2021, with 732 and 30.03%, respectively. This indicates that the patch shape of mangrove forests was complex as the NP increased. LPI and AI also fluctuated from an increase to a decrease several times, with LPI reaching at least 6.42 in 2021. In conclusion, the edge shape of the mangrove patch in the Hainan Island in 2021 is complex, with low connectivity and substantial fragmentation. At the city and county levels, only Haikou City and Dongfang City displayed relatively reduced landscape fragmentation and strong landscape connectivity by 2021.

The spatial distribution of the surface cover area of the mangrove forest crown in the 12 cities and counties along the coast of the Hainan Island was used to investigate the path of mass center offsets across the six periods. From 1991 to 2021, most centers of the mangrove forest mass in the Hainan Island showed a trend of coastal movement toward the ocean or inlets, the distance of movement in the first stage being the largest (Figure 9). Specifically, the mass center of Changjiang Li Autonomous County moved in a unidirectional line, as mangrove forests were only positively identified in two of the analysis years; moreover, the mass centers of the mangrove forests in Sanya, Danzhou, and Wanning cities also moved unidirectionally until 2021, when they showed a folded-back trend. The movement trajectories in all the remaining locations appeared circular or crossed and overlapped, indicating the factors influencing mangrove forest survival.
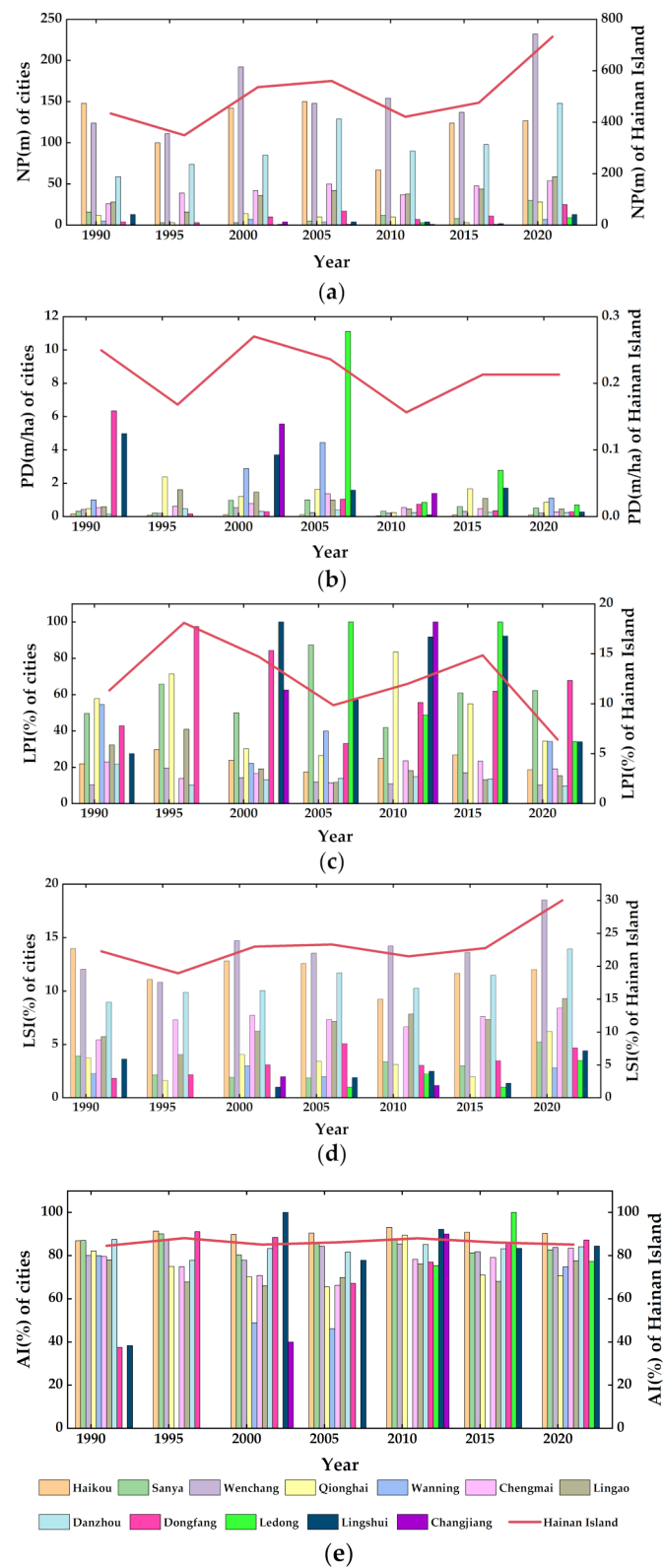
Figure 8. Landscape pattern index of mangrove forests in the Hainan Island during 1991–2021. (**a**) NP (m) index; (**b**) PD (m/ha) index; (**c**) LPI (%) index; (**d**) LSI (%) index; (**e**) AI (%) index.
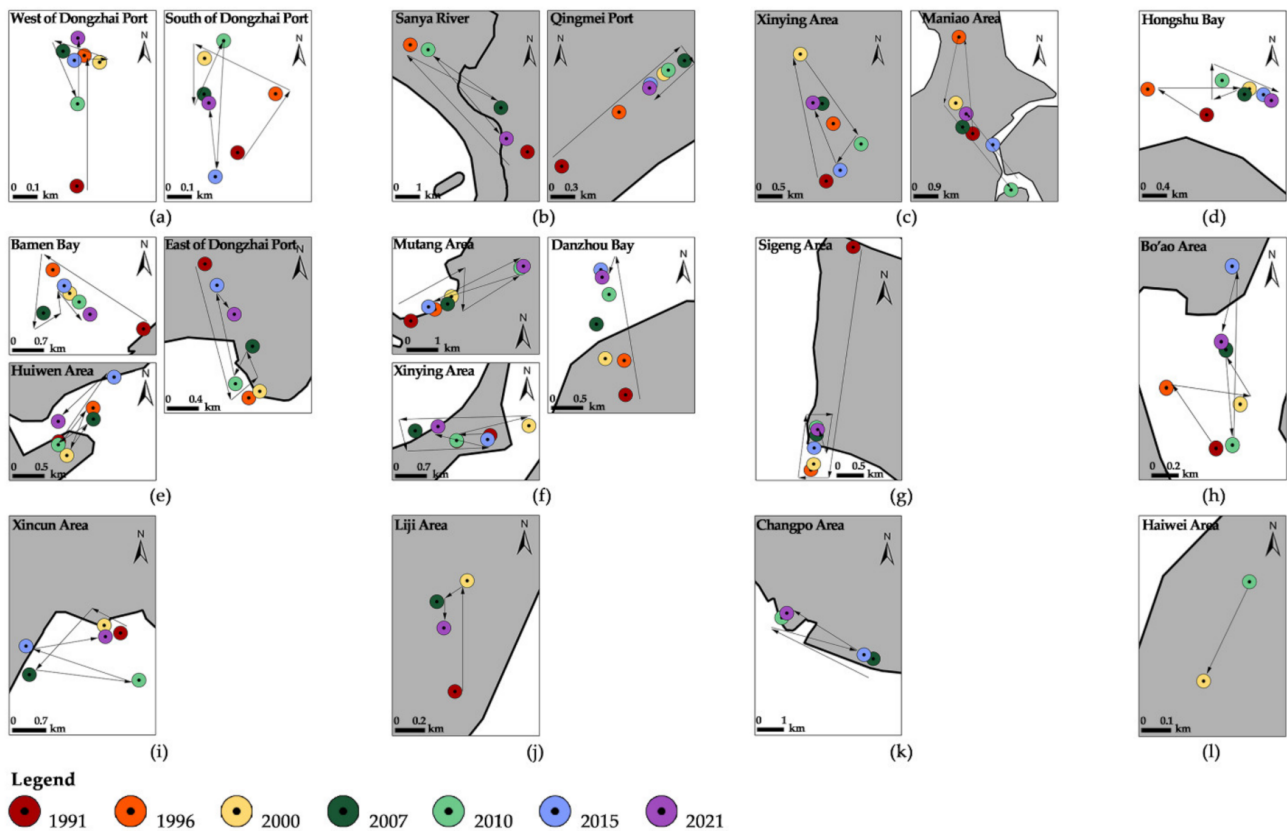
Figure 9. Mass center offset maps of mangrove forests across the Hainan Island for (**a**) Haikou, (**b**) Sanya, (**c**) Lingao, (**d**) Chengmai, (**e**) Wenchang, (**f**) Danzhou, (**g**) Dongfang, (**h**) Qionghai, (**i**) Lingshui, (**j**) Wanning, (**k**) Ledong, and (**l**) Changjiang.

3.2.3. Influential Mechanisms of Mangrove Forest Landscape Evolution

From 1991 to 2021, the total and urban populations of the Hainan Island grew continuously, whereas the rural population slowly decreased. Furthermore, the GDP of the island increased from 10.793 billion yuan in 1991 to 553.229 billion yuan in 2021, from which the value of fishery rose from 836 million yuan to 39.080 billion yuan (Figure 10). However, the overall patterns of average annual rainfall and minimum and maximum temperatures throughout the study period were complex, although all increased (Table 6).
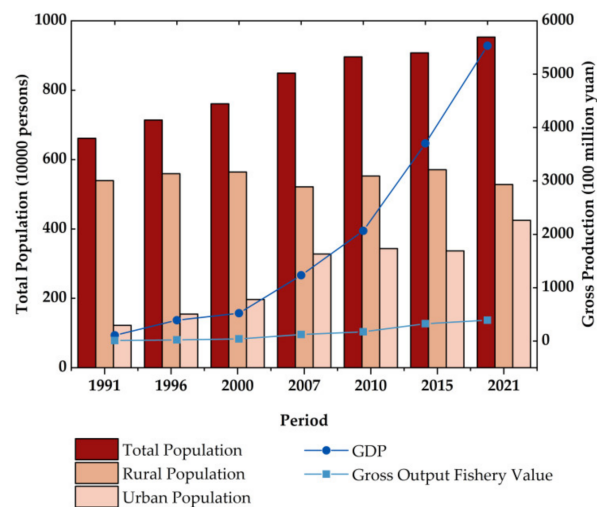
Figure 10. Population and socioeconomic development dynamics of the Hainan Island during 1991–2021.

Table 6. Climate and environmental indicator dynamics in the Hainan Island during 1991–2021.

Period	Average Annual Rainfall (mm)	Average Annual Minimum Temperature (°C)	Average Annual Maximum Temperature (°C)
1991	1289.12	21.65	28.5
1996	1531.08	21.12	27.68
2000	1804.22	21.6	27.76
2007	1334.88	21.72	28.01
2010	1507.96	21.45	27.88
2015	1554.69	22.27	28.66
2021	1548.06	22.44	29.11
Linear Fit	$y = 18.849x + 1434.6$	$y = 0.1614x + 21.104$	$y = 0.1396x + 27.67$
R^2	$R^2 = 0.0585$	$R^2 = 0.5760$	$R^2 = 0.3163$

According to the correlation analyses with mangrove forest crown surface cover areas in the Hainan Island (Table 7), positive correlations were observed with the socioeconomic factors of the total population, GDP, and the gross output value of fisheries ($p < 0.05$). Moreover, the change in the surface cover of the mangrove forest crown showed a significant positive correlation with the urban population ($p < 0.01$). Specifically, in the correlation analysis of the mangrove forest crown surface cover area change in each city and county, Wenchang City and Lingshui Li Autonomous County showed a significant positive correlation between mangrove forest crown surface cover area and urban population; the growth of the mangrove forest crown surface cover area in Wenchang City, Chengmai County, Lingao County, Danzhou City, Dongfang City, and Ledong Li Autonomous County displayed significant positive correlations with the local GDP; whereas that of Chengmai County showed a highly significant positive correlation with both GDP and the gross output value of fisheries. Regarding climatic factors, all correlations with the mangrove forest crown surface cover area across the Hainan Island were positive but weak; however, analyses at city and county levels found that the crown surface cover area changes in Chengmai County and Danzhou City were significantly positively correlated with both the average annual minimum and maximum temperatures.

Table 7. Pearson correlation analysis results of mangrove forest crown surface cover area with socioeconomic and climatic factors over the Hainan Island during 1991–2021.

City/County	Total Pop [1]	Rural Pop.	Urban Pop.	GDP	Gross Output Fishery Value	Average Annual Rainfall	Average Annual Minimum Temperature	Average Annual Maximum Temperature
Hainan Island	0.836 *	−0.42	0.875 **	0.853 *	0.801 *	0.09	0.56	0.52
Haikou	0.51	0.37	0.49	0.19	0.29	0.28	−0.16	−0.37
Sanya	0.21	−0.70	0.39	0.47	0.30	−0.48	0.33	0.63
Wenchang	0.72	−0.764 *	0.901 **	0.797 *	0.788 *	0.11	0.35	0.41
Qionghai	0.29	0.14	0.18	0.28	0.21	−0.04	0.07	0.24
Wanning	−0.15	−0.52	0.15	0.27	0.23	−0.20	0.44	0.63
Chengmai	0.61	−0.775 *	0.73	0.922 **	0.885 **	0.21	0.767 *	0.797 *
Lingao	0.59	0.57	0.58	0.772 *	0.71	−0.14	0.66	0.73
Danzhou	0.53	0.51	0.47	0.800 *	0.75	−0.15	0.842 *	0.867 *
Dongfang	0.57	−0.30	0.73	0.770 *	0.64	0.49	0.71	0.62
Ledong	0.62	0.58	0.40	0.810 *	0.67	0.00	0.63	0.64
Lingshui	0.60	−0.40	0.825 *	0.69	0.62	−0.03	0.39	0.38
Changjiang	0.19	0.49	−0.01	−0.17	−0.21	0.62	−0.16	−0.47

[1] Pop. refers to the population; * $p < 0.05$; ** $p < 0.01$.

4. Discussion

4.1. Comparative Analysis of Mangrove Classification Methods

In this study, the accuracy of the SVM and Res-UNet algorithms used to identify the distribution range of mangrove forests in the Hainan Island from 1991 to 2021 produced OA values of 93.11 ± 1.54% and 96.43 ± 1.15%, respectively; the PA of Res-UNet was resultantly much greater than SVM. It was observed that the Res-UNet algorithm based on

a convolutional neural network produced a higher correct classification rate for the crown surface cover area of the mangrove forest.

In their examination of the Pichavaram mangrove wetland that spans 2335.5 ha, Singh et al. [43] achieved the highest overall classification accuracy by using an SVM to identify mangrove images (94.53%). Zhen et al. [27] used an SVM to classify the land use of the Dongzhai Port National Nature Reserve in Hainan, finding that OA could reach 83.5%; thus, it has been shown that SVMs can delineate the distributions of mangrove forests in small-scale wetland parks or natural reserves. Similarly, this study found that SVM can effectively extract the land area of mangrove forests in the Hainan Island, which has the advantage of identifying mangrove forest land areas at a large scale.

However, the SVM algorithm often failed to accurately distinguish spectrally similar mangrove forests from aquatic herbs and water surfaces. Hu et al. [19] found that spectral-temporal variability metrics could distinguish mangrove forests from agricultural fields or other natural terrestrial vegetation with high spectral similarity, but some aquatic plants were still misclassified. Alternatively, Jia et al. [44] used K-nearest neighbor (KNN) for object-based classification; however, mangrove forests were still incorrectly distinguished from water surfaces. Thus, the results show that machine-learning algorithms have yet to clearly resolve the misclassification problem of mangrove forest land cover classifications.

In the ground survey of mangrove forests on the Hainan Island, in areas with high mangrove mortality, the local government would usually plant mangrove seedlings frequently, which caused the mangrove forests in most areas to be at the seedling stage. However, Landsat satellite data with a 30 m spatial resolution were not effective in identifying mangrove forests at the seedling stage, which caused the mangrove forest land area identified by SVM and the mangrove crown surface cover identified by Res-UNet to be smaller than the studies of Hu et al. [19] and Jia et al. [44] (Table 8). Furthermore, the area of the mangrove crown surface cover identified by Res-UNet was more detailed and could better reflect the characteristics of the distribution of the patches of mangrove forests while offering more advantages for analyzing the fragmentation of mangrove forests. The Res-UNet deep learning not only produced a high OA but also significantly reduced misclassifications. Specifically, most of the mixed pixels containing spectrally similar aquatic plants and water surfaces to the mangrove forests were correctly separated by this algorithm. Therefore, in mangrove areas difficult to access in the surface cover of the ground survey, the mangrove forest crown could be obtained with the help of Res-UNet deep learning. The Res-UNet is more effective in identifying a large-scale area of mangrove crown surface cover area. In addition, the mangrove forest crown surface cover area is helpful for us to explore changes in mangrove biomass and carbon storage.

Table 8. Comparison of mangrove forest areas in the Hainan Island among different studies.

Name	Classification Algorithm	Mangrove Forests Area (ha)						
		1991	1996	2000	2007	2010	2015	2021
Mangrove forest land area in this study	SVM	3081	2917	2851	3030	3072	3493	3827
Mangrove forests crown surface cover area in this study	Res-UNet	1740	2077	1985	2372	2695	2234	3439
Mangrove forest land area Hu et al. [19]	RF	1990	1995	2000	2005	2010	2015	
		3701	3141	3235	3305	3623	3702	
Mangrove forest land area Jia et al. [44]	KNN	1990		2000		2010	2015	
		4809		3978		3576	4017	

4.2. Spatiotemporal Evolution of Mangrove Forests in the Hainan Island

During 1991–2021, the total area of the mangrove forest crown surface coverage on the Hainan Island showed a net increase of 1698.48 ha, corresponding to an annual change rate of 2.27%·yr^{-1}. Related studies have shown that since the early 1990s, China has paid increasing attention to wetland conservation, with the government enacting a series of

corresponding protective laws and regulations, including the China Biodiversity Conservation Action Plan (State Environmental Protection Administration, 1994), Agenda 21 Forestry Action Plan (State Forestry Administration, 1995; 1996), Ecological Environmental Protection Plan (State Council, 1998), and the Wetland Conservation Action Plan (State Forestry Administration, 2000) [42]. Combining the change in center mass, population trends, and socioeconomic developments in the Hainan Island, it was further revealed that mangrove forests near landed areas were rapidly decreasing and expanding to the mudflats by the sea due to population growth and urbanization.

This study revealed that in both 2000 and 2015, the area of the mangrove forest crown surface cover on the Hainan Island decreased, NP increased, and both LPI and AI decreased, indicative of the continued deterioration and fragmentation of the mangrove forest connectivity during these two phases. Changes in LSI indicated that landscape shape complexity was also increasing. With the gradual progress of urbanization, the interference of human activities on the landscape pattern also proved to be increasing; therefore, in landscape pattern evolution, fragmentation levels are growing, leading to the increased complexity of landscape patches. Although the area of the mangrove forest crown surface cover in the Hainan Island has increased over the past three decades largely due to the intensification of mangrove forest restoration efforts, negative growth occurred approximately every 10 to 15 years throughout the study period. Especially in 2015, the crown surface cover area of the mangrove forest on the Hainan Island decreased significantly. However, in six years, it added more than a thousand hectares. The reason for this can be found in the Annual Statistical Report of the Hainan Province. From 2015 to 2021, the total area of shelter forests planted on the Hainan Island reached 14,661 hectares. This shows that the increase in planted mangrove forests based on conservation strategies and the decrease in naturally occurring mangrove forests may cause increased landscape fragmentation, and the landscape shape is single. Furthermore, the survival rate of artificially planted mangrove forests is low [44], indicating a relatively low overall conservation efficiency. Therefore, future mangrove protection and management should be based on protection and supplemented by restoration, as maintaining the current health of existing mangrove ecosystems to improve their resilience is usually more time efficient and economical than planting large amounts of new mangrove forests [45].

Spatially, the arial changes in the mangrove forest crown surface cover observed in each city or county over the 30-year analysis period followed the overall growth trends. In addition, the landscape patterns in Haikou and Danzhou cities showed a significant improvement. According to the preliminary analysis, this results from the excellent landscape patterns in these cities due to the presence of mangrove nature reserves [46]. The expansion of the mangrove forest crown surface coverage in the Hainan Island was positively correlated with the development of the whole island economy, fishery production, and expanding urban population. This suggests that the mangrove forest crown surface cover area in the Hainan Island will increase as the rural population shifts toward urban areas with greater socioeconomic development. The rapid development of this tertiary industry and the shift of the rural population to cities have reduced the damage to mangrove forests caused by agricultural practices, such as constructing coastal lands. Furthermore, because mangrove forests maintain their natural purification ability and can provide a constant source of organic debris and other food sources for benthic organisms, organized fish farming activities may play a certain role in promoting the growth of mangrove forest areas. Therefore, the local government and residents' awareness of mangrove forest protection should be increased while focusing on maintaining the ecological environment of mangrove forests; furthermore, the benefits of resources should be optimized for sustainable fish farming, so a synergistic effect between ecological protection and economic development can be achieved.

5. Conclusions

Using Landsat imagery data in this study alongside employed machine-learning (SVM) and deep learning algorithms (Res-UNet) to extract information from tropical mangrove forests meant that the accuracy of these two methods could be analyzed and compared. The OA for the extraction of the mangrove forest spatial distribution extraction produced values of 93.11 ± 1.54 and 96.43 ± 15% for SVM and Res-UNet, respectively. The superior classification results were produced by the deep learning algorithm compared to machine learning, as the proposed model of Res-UNet combined a semantic segmentation network (U-Net) and the feature extraction network ResNet-18. This method effectively resolved previous issues regarding the misclassification of spectrally similar pixels in large-scale study areas. Moreover, the Res-UNet algorithm was more efficient and accurate at extracting the crown surface cover area of mangrove forests, providing an important foundation for the refined calculation of the carbon sequestration potential for these forests.

The present study analyzed the spatiotemporal changes in the tropical mangrove landscape patterns on the Hainan Island over the past 30 years from multiple perspectives, including the corresponding changes in crown surface cover, landscape fragmentation, mass centering offsets, as well as anthropogenic and climatic factors. The results revealed that mangrove forests in most areas underwent an overall trend of growth. Although there were various spatial differences among cities and counties, the recorded changes to the mangrove forests were mainly influenced by an increase in landscape fragmentation due to human disturbance. Additionally, this study assessed the relationships between changes to the tropical mangrove forested land area or crown surface coverage as responses to mechanisms of shifting climate and socioeconomic factors across the Hainan Island. Although this study focused on the socioeconomic factors affecting mangrove forest dynamics, and climatic and environmental factors, it also investigated how these factors contributed to these corresponding changes. For example, it was found that the average annual rainfall, as well as average annual minimum and maximum temperatures, were positively correlated with mangrove forest crown surface cover area changes in the Hainan Island; however, these correlations were not significant. Only the growth of mangrove forests in Chengmai County and Danzhou City was significantly correlated with climatic factors. Because, compared with human activity disturbances, the process of climate factors affecting mangrove wetlands has an inherent lag component, the impacts of more gradual environmental changes on mangrove ecosystems appear relatively insignificant [47]. Furthermore, the strong interference of human activities makes the evolutionary mechanisms that affect mangrove landscapes highly complex; therefore, it is necessary to obtain additional data related to the influencing factors for in-depth analyses. Therefore, more field surveys and remote sensing monitoring data are required to further study the integrated driving forces of mangrove forest dynamics. More detailed and perfect suggestions must be presented for mangrove forest nature reserve-related landscape planning to provide more appropriate ideas for tropical mangrove forest protection.

Conflicts of Interest: The authors declare no conflict of interest.

Appendix A

Appendix A.1

In this study, a handheld GPS and Google Earth were used to survey the main distribution areas of the mangrove forests in 12 cities and counties along the coast of the Hainan Island in October 2021. The dominant tree species in each city are shown in Table A1.

Table A1. Information on dominant tree species of mangrove forests in the Hainan Island obtained from a ground survey.

Distribution of Dominant Mangrove Forests Tree Species in Hainan Island, 2021	
City/County	**Tree Species**
Haikou	*Acanthus ilicifolius* L. *Acrostichum speciosum* Will. *Aegiceras corniculatum* (Linn.) Blanco *Avicennia marina* (Forsk) Vierh. *Bruguiera gymnorrhiza* (Linn.) Sav. *Bruguiera sexangula* (Lour.) Poir. *Bruguiera sexangula* (Lour.) Poir. var. *rhynchopetala* Ko *Ceriops tagal* (Perr.) C. B. Rob. *Excoecaria agallocha* Linn. *Hibiscus tiliaceus* Linn. *Kandelia obovata* Sheue, Liu et Yong *Laguncularia racemosa* Gaertn. f. *Pongamia pinnata* (Linn.) Pierre *Rhizophora apiculata* Blume *Rhizophora stylosa* Griff *Sonneratia apetala* Buch. -Ham.
Sanya	*Aegiceras corniculatum* (Linn.) Blanco *Avicennia marina* (Forsk) Vierh. *Ceriops tagal* (Perr.) C. B. Rob. *Lumnitzera racemosa* Willd *Rhizophora apiculata* Blume *Rhizophora stylosa* Griff. *Sonneratia* × *hainanensis* Ko, E. Y. Chen et W. Y. Chen *Sonneratia alba* J. Smith *Sonneratia ovata* Backer *Xylocarpus granatum* J. Koenig
Wenchang	*Avicennia marina* (Forsk) Vierh. *Bruguiera gymnorrhiza* (Linn.) Sav. *Bruguiera sexangula* (Lour.) Poir. var. *rhynchopetala* Ko *Ceriops tagal* (Perr.) C. B. Rob. *Excoecaria agallocha* Linn. *Hibiscus tiliaceus* Linn. *Kandelia obovata* Sheue, Liu et Yong *Laguncularia racemosa* Gaertn. f. *Lumnitzera littorea* (Jack) Voigt *Rhizophora apiculata* Blume *Rhizophora stylosa* Griff. *Sonneratia* × *hainanensis* Ko, E. Y. Chen et W. Y. Chen *Sonneratia alba* J. Smith *Sonneratia caseolaris* (Linn.) Engl. *Sonneratia ovata* Backer
Qionghai	*Bruguiera gymnorrhiza* (Linn.) Sav. *Cerbera manghas* L. *Hibiscus tiliaceus* Linn. *Sonneratia* × *hainanensis* Ko, E. Y. Chen et W. Y. Chen *Sonneratia alba* J. Smith *Sonneratia ovata* Backer
Wanning	*Bruguiera gymnorrhiza* (Linn.) Sav. *Cerbera manghas* L. *Excoecaria agallocha* Linn. *Hibiscus tiliaceus* Linn. *Nypa fruticans* Wurmb. *Sonneratia caseolaris* (Linn.) Engl.
Chengmai	*Aegiceras corniculatum* (Linn.) Blanco *Avicennia marina* (Forsk) Vierh. *Hibiscus tiliaceus* Linn. *Kandelia obovata* Sheue, Liu et Yong *Lumnitzera littorea* (Jack) Voigt *Rhizophora apiculata* Blume *Rhizophora stylosa* Griff. *Sonneratia caseolaris* (Linn.) Engl.
Lingao	*Aegiceras corniculatum* (Linn.) Blanco *Avicennia marina* (Forsk) Vierh. *Excoecaria agallocha* Linn. *Hibiscus tiliaceus* Linn. *Rhizophora stylosa* Griff.
Danzhou	*Aegiceras corniculatum* (Linn.) Blanco *Avicennia marina* (Forsk) Vierh. *Hibiscus tiliaceus* Linn. *Kandelia obovata* Sheue, Liu et Yong *Lumnitzera littorea* (Jack) Voigt *Rhizophora stylosa* Griff.
Dongfang	*Avicennia marina* (Forsk) Vierh. *Laguncularia racemosa* Gaertn. f.
Ledong	*Rhizophora stylosa* Griff. *Lumnitzera littorea* (Jack) Voigt *Avicennia marina* (Forsk) Vierh. *Laguncularia racemosa* Gaertn. f.

Table A1. *Cont.*

Distribution of Dominant Mangrove Forests Tree Species in Hainan Island, 2021	
City/County	**Tree Species**
Lingshui	*Avicennia marina* (Forsk) Vierh. *Rhizophora stylosa* Griff. *Bruguiera gymnorrhiza* (Linn.) Sav. *Sonneratia* × *hainanensis* Ko, E. Y. Chen et W. Y. Chen *Bruguiera sexangula* (Lour.) Poir. var. *rhynchopetala* Ko *Sonneratia alba* J. Smith *Kandelia obovata* Sheue, Liu et Yong *Sonneratia apetala* Buch. -Ham. *Laguncularia racemosa* Gaertn. f. *Sonneratia ovata* Backer
Changjiang	*Avicennia marina* (Forsk) Vierh. *Rhizophora stylosa* Griff

Appendix A.2

Figure A1 indicates the classification results of the SVM machine-learning algorithm, and Figure A2 indicates the classification results of the Res-UNet deep learning algorithm.

(a)

(b)

(c)
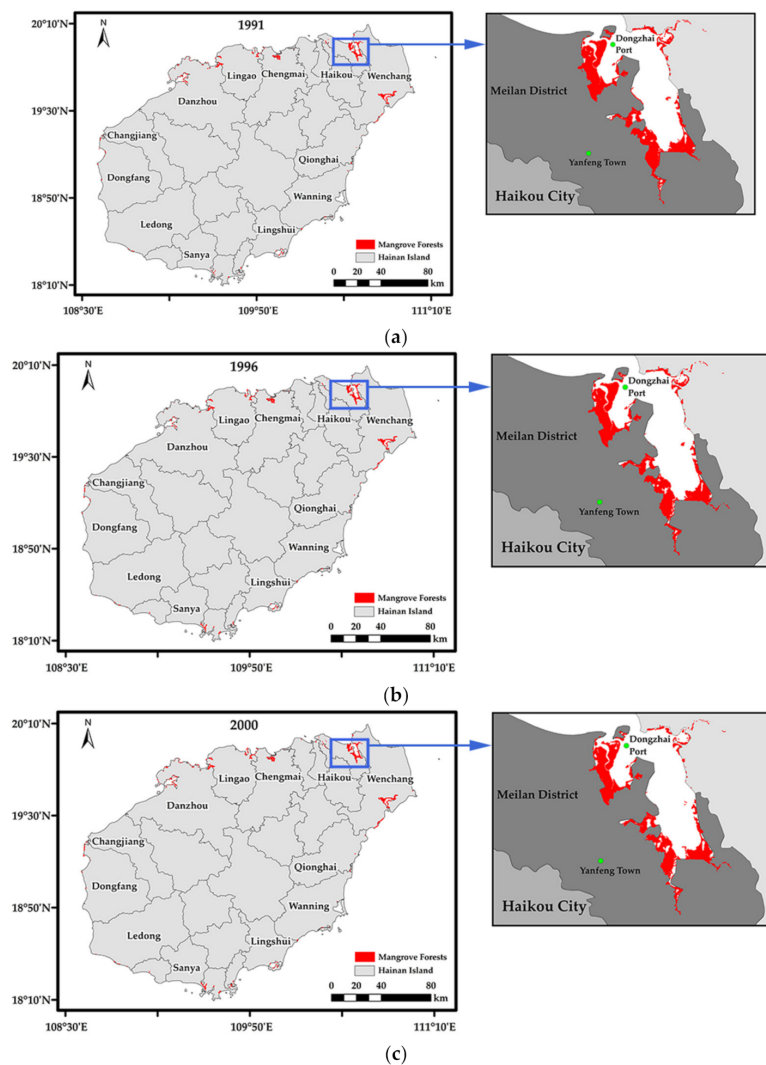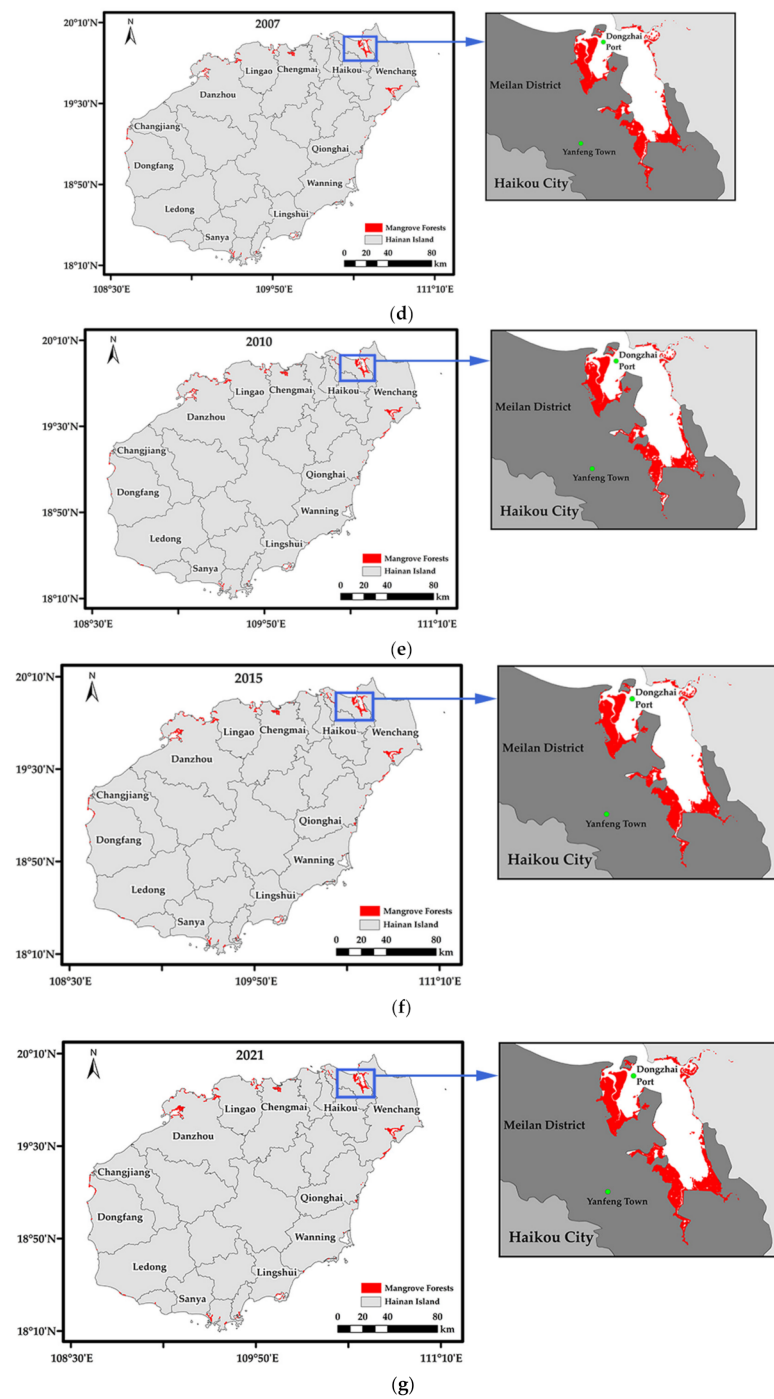
Figure A1. *Cont.*

Figure A1. SVM machine-learning classification results. (**a**) 1991; (**b**) 1996; (**c**) 2000; (**d**) 2007; (**e**) 2010; (**f**) 2015; (**g**) 2021.
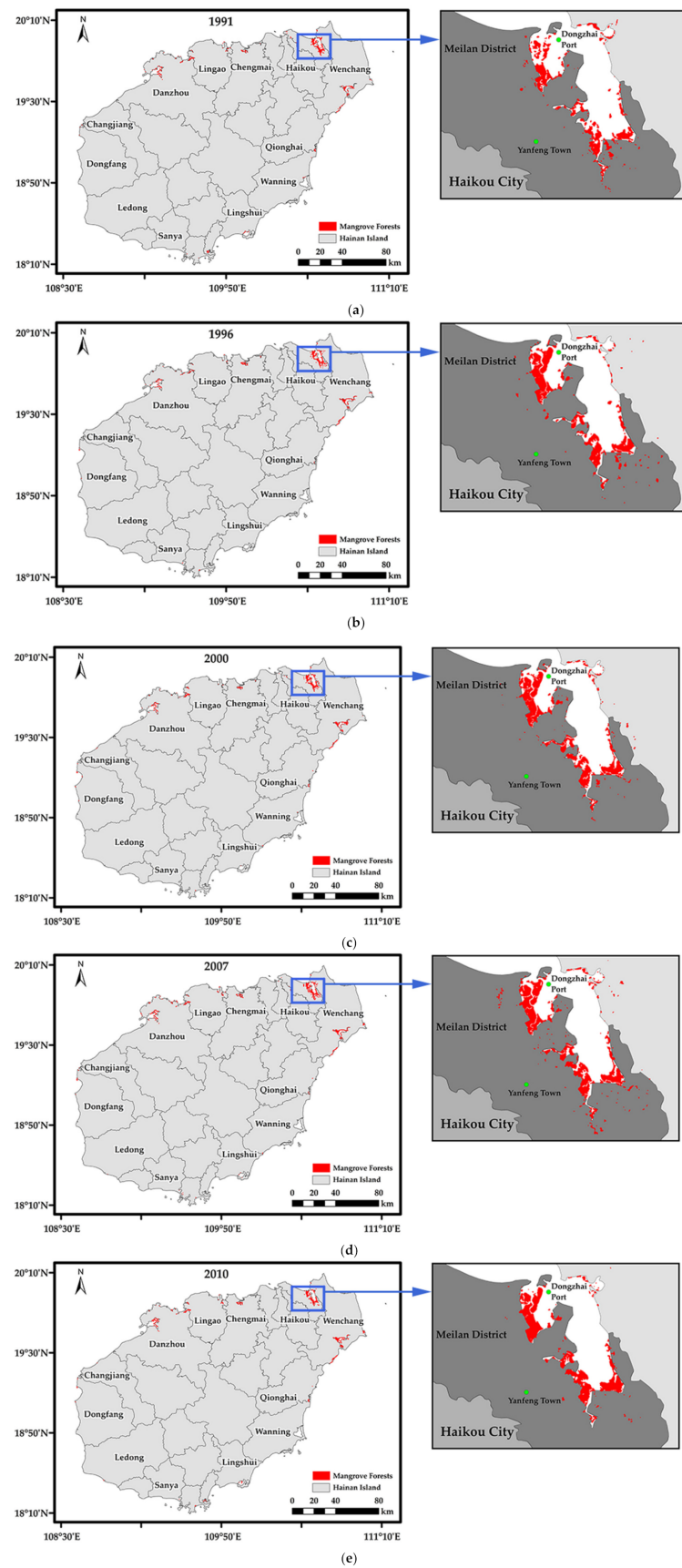
Figure A2. *Cont*.
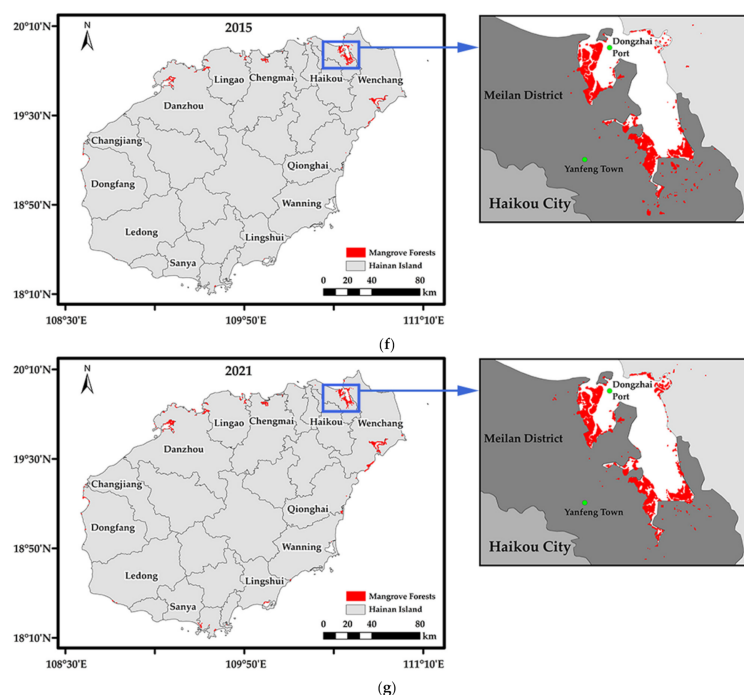
Figure A2. Classification results of Res-UNet machine-learning. (**a**) 1991; (**b**) 1996; (**c**) 2000; (**d**) 2007; (**e**) 2010; (**f**) 2015; (**g**) 2021.

References

1. Tomlinson, P.B. *The Botany of Mangroves*; Cambridge University Press: Cambridge, MA, USA, 2016.
2. Simard, M.; Fatoyinbo, L.; Smetanka, C.; Rivera-Monroy, V.H.; Castañeda-Moya, E.; Thomas, N.; Van der Stocken, T. Mangrove canopy height globally related to precipitation, temperature and cyclone frequency. *Nat. Geosci.* **2019**, *12*, 40–45. [CrossRef]
3. Getzner, M.; Islam, M.S. Ecosystem services of mangrove forests: Results of a meta-analysis of economic values. *Int. J. Environ. Res. Public Health* **2020**, *17*, 5830. [CrossRef] [PubMed]
4. Donato, D.C.; Kauffman, J.B.; Murdiyarso, D.; Kurnianto, S.; Stidham, M.; Kanninen, M. Mangroves among the most carbon-rich forests in the tropics. *Nat. Geosci.* **2011**, *4*, 293–297. [CrossRef]
5. Lee, S.Y.; Primavera, J.H.; Dahdouh-Guebas, F.; McKee, K.; Bosire, J.O.; Cannicci, S.; Diele, K.; Fromard, F.; Koedam, N.; Marchand, C. Ecological role and services of tropical mangrove ecosystems: A reassessment. *Glob. Ecol. Biogeogr.* **2014**, *23*, 726–743. [CrossRef]
6. Goldberg, L.; Lagomasino, D.; Thomas, N.; Fatoyinbo, T. Global declines in human-driven mangrove loss. *Glob. Chang. Biol.* **2020**, *26*, 5844–5855. [CrossRef]
7. Friess, D.A.; Rogers, K.; Lovelock, C.E.; Krauss, K.W.; Hamilton, S.E.; Lee, S.Y.; Lucas, R.; Primavera, J.; Rajkaran, A.; Shi, S. The state of the world's mangrove forests: Past, present, and future. *Annu. Rev. Environ. Resour.* **2019**, *44*, 89–115. [CrossRef]
8. Murray, N.J.; Phinn, S.R.; DeWitt, M.; Ferrari, R.; Johnston, R.; Lyons, M.B.; Clinton, N.; Thau, D.; Fuller, R.A. The global distribution and trajectory of tidal flats. *Nature* **2019**, *565*, 222–225. [CrossRef]
9. Wang, L.; Jia, M.; Yin, D.; Tian, J. A review of remote sensing for mangrove forests: 1956–2018. *Remote Sens. Environ.* **2019**, *231*, 111223. [CrossRef]
10. Liu, X.; Yang, X.; Zhang, T.; Wang, Z.; Zhang, J.; Liu, Y.; Liu, B. Remote sensing based conservation effectiveness evaluation of mangrove reserves in china. *Remote Sens.* **2022**, *14*, 1386. [CrossRef]
11. Purnamasayangsukasih, P.R.; Norizah, K.; Ismail, A.A.; Shamsudin, I. A review of uses of satellite imagery in monitoring mangrove forests. Proceeding of 8th IGRSM International Conference and Exhibition on Geospatial & Remote Sensing (IGRSM 2016), Kuala Lumpur, Malaysia, 13–14 April 2016; 37, p. 012034. [CrossRef]
12. Hauser, L.T.; Vu, G.N.; Nguyen, B.A.; Dade, E.; Nguyen, H.M.; Nguyen, T.T.Q.; Le, T.Q.; Vu, L.H.; Tong, A.T.H.; Pham, H.V. Uncovering the spatio-temporal dynamics of land cover change and fragmentation of mangroves in the Ca Mau peninsula, Vietnam using multi-temporal SPOT satellite imagery (2004–2013). *Appl. Geogr.* **2017**, *86*, 197–207. [CrossRef]
13. Proisy, C.; Viennois, G.; Sidik, F.; Andayani, A.; Enright, J.A.; Guitet, S.; Gusmawati, N.; Lemonnier, H.; Muthusankar, G.; Olagoke, A. Monitoring mangrove forests after aquaculture abandonment using time series of very high spatial resolution satellite images: A case study from the perancak estuary, bali, indonesia. *Mar. Pollut. Bull.* **2018**, *131*, 61–71. [CrossRef] [PubMed]
14. Pham, T.D.; Xia, J.; Ha, N.T.; Bui, D.T.; Le, N.N.; Takeuchi, W. A review of remote sensing approaches for monitoring blue carbon ecosystems: Mangroves, seagrasses and salt marshes during 2010–2018. *Sensors* **2019**, *19*, 1933. [CrossRef] [PubMed]
15. Gaw, L.Y.; Linkie, M.; Friess, D.A. Mangrove forest dynamics in tanintharyi, myanmar from 1989–2014, and the role of future economic and political developments. *Singap. J. Trop. Geogr.* **2018**, *39*, 224–243. [CrossRef]

16. Hu, L.; Li, W.; Xu, B. The role of remote sensing on studying mangrove forest extent change. *Int. J. Remote Sens.* **2018**, *39*, 6440–6462. [CrossRef]

17. Thakur, S.; Mondal, I.; Ghosh, P.; Das, P.; De, T. A review of the application of multispectral remote sensing in the study of mangrove ecosystems with special emphasis on image processing techniques. *Spat. Inf. Res.* **2020**, *28*, 39–51. [CrossRef]

18. Buck, O.; Millán, V.E.G.; Klink, A.; Pakzad, K. Using information layers for mapping grassland habitat distribution at local to regional scales. *Int. J. Appl. Earth Obs. Geoinf.* **2015**, *37*, 83–89. [CrossRef]

19. Hu, L.; Li, W.; Xu, B. Monitoring mangrove forest change in china from 1990 to 2015 using landsat-derived spectral-temporal variability metrics. *Int. J. Appl. Earth Obs. Geoinf.* **2018**, *73*, 88–98. [CrossRef]

20. Abdi, A.M. Land cover and land use classification performance of machine learning algorithms in a boreal landscape using sentinel-2 data. *GIScience Remote Sens.* **2020**, *57*, 1–20. [CrossRef]

21. Guo, Y.; Liao, J.; Shen, G. Mapping large-scale mangroves along the maritime silk road from 1990 to 2015 using a novel deep learning model and landsat data. *Remote Sens.* **2021**, *13*, 245. [CrossRef]

22. Li, H.; Hu, B.; Li, Q.; Jing, L. Cnn-based individual tree species classification using high-resolution satellite imagery and airborne lidar data. *Forests* **2021**, *12*, 1697. [CrossRef]

23. Zhang, Z.; Liu, Q.; Wang, Y. Road extraction by deep residual u-net. *IEEE Geosci. Remote Sens. Lett.* **2018**, *15*, 749–753. [CrossRef]

24. Cao, K.; Zhang, X. An improved res-unet model for tree species classification using airborne high-resolution images. *Remote Sens.* **2020**, *12*, 1128. [CrossRef]

25. Ibharim, N.; Mustapha, M.; Lihan, T.; Mazlan, A. Mapping mangrove changes in the matang mangrove forest using multi temporal satellite imageries. *Ocean Coast. Manag.* **2015**, *114*, 64–76. [CrossRef]

26. Son, N.T.; Thanh, B.X.; Da, C.T. Monitoring mangrove forest changes from multi-temporal landsat data in can gio biosphere reserve, vietnam. *Wetlands* **2016**, *36*, 565–576. [CrossRef]

27. Zhen, J.; Liao, J.; Shen, G. Mapping mangrove forests of dongzhaigang nature reserve in china using landsat 8 and radarsat-2 polarimetric sar data. *Sensors* **2018**, *18*, 4012. [CrossRef]

28. Gilani, H.; Naz, H.I.; Arshad, M.; Nazim, K.; Akram, U.; Abrar, A.; Asif, M. Evaluating mangrove conservation and sustainability through spatiotemporal (1990–2020) mangrove cover change analysis in pakistan. *Estuar. Coast. Shelf Sci.* **2021**, *249*, 107128. [CrossRef]

29. Giri, C.; Long, J.; Abbas, S.; Murali, R.M.; Qamer, F.M.; Pengra, B.; Thau, D. Distribution and dynamics of mangrove forests of south asia. *J. Environ. Manag.* **2015**, *148*, 101–111. [CrossRef]

30. Liao, J.; Zhen, J.; Zhang, L.; Metternicht, G. Understanding dynamics of mangrove forest on protected areas of hainan island, china: 30 years of evidence from remote sensing. *Sustainability* **2019**, *11*, 5356. [CrossRef]

31. Vapnik, V. *The Nature of Statistical Learning Theory*; Springer Science & Business Media: Berlin/Heidelberg, Germany, 1999.

32. Maxwell, A.E.; Warner, T.A.; Fang, F. Implementation of machine-learning classification in remote sensing: An applied review. *Int. J. Remote Sens.* **2018**, *39*, 2784–2817. [CrossRef]

33. Ronneberger, O.; Fischer, P.; Brox, T. In U-net: Convolutional networks for biomedical image segmentation. In Proceedings of the International Conference on Medical Image Computing and Computer-Assisted Intervention, Munich, Germany, 5–9 October 2015; Springer: Berlin/Heidelberg, Germany, 2015; pp. 234–241. Available online: https://lmb.informatik.uni-freiburg.de/people/ronneber/u-net/ (accessed on 1 September 2022).

34. He, K.; Zhang, X.; Ren, S.; Sun, J. Deep residual learning for image recognition. In Proceedings of the IEEE Conference on Computer Vision and Pattern Recognition, Las Vegas, NV, USA, 27–30 June 2016; pp. 770–778. Available online: https://openaccess.thecvf.com/content_cvpr_2016/html/He_Deep_Residual_Learning_CVPR_2016_paper.html (accessed on 1 September 2022).

35. Chaurasia, A.; Culurciello, E. Linknet: Exploiting encoder representations for efficient semantic segmentation. In Proceedings of the 2017 IEEE Visual Communications and Image Processing (VCIP), St. Petersburg, FL, USA, 10–13 December 2017; pp. 1–4. [CrossRef]

36. Kingma, D.P.; Ba, J. Adam: A method for stochastic optimization. *arXiv* **2014**, arXiv:1412.6980. [CrossRef]

37. Anand, A. *Unit-14 Accuracy Assessment. Processing and Classification of Remotely Sensed Images. Remote Sensing and Image Interpretaion*; Indiara Gandhi National Open University: Delhi, India, 2017; pp. 59–78.

38. Puyravaud, J.-P. Standardizing the calculation of the annual rate of deforestation. *For. Ecol. Manag.* **2003**, *177*, 593–596. [CrossRef]

39. Zhang, J.; Yang, X.; Wang, Z.; Zhang, T.; Liu, X. Remote sensing based spatial-temporal monitoring of the changes in coastline mangrove forests in china over the last 40 years. *Remote Sens.* **2021**, *13*, 1986. [CrossRef]

40. Fu, F.; Deng, S.; Wu, D.; Liu, W.; Bai, Z. Research on the spatiotemporal evolution of land use landscape pattern in a county area based on ca-markov model. *Sustain. Cities Soc.* **2022**, *80*, 103760. [CrossRef]

41. Li, H.; Man, W.; Li, X.; Ren, C.; Wang, Z.; Li, L.; Jia, M.; Mao, D. Remote sensing investigation of anthropogenic land cover expansion in the low-elevation coastal zone of liaoning province, china. *Ocean Coast. Manag.* **2017**, *148*, 245–259. [CrossRef]

42. Zheng, Y.; Takeuchi, W. Quantitative assessment and driving force analysis of mangrove forest changes in china from 1985 to 2018 by integrating optical and radar imagery. *ISPRS Int. J. Geo-Inf.* **2020**, *9*, 513. [CrossRef]

43. Singh, S.K.; Srivastava, P.K.; Gupta, M.; Thakur, J.K.; Mukherjee, S. Appraisal of land use/land cover of mangrove forest ecosystem using support vector machine. *Environ. Earth Sci.* **2014**, *71*, 2245–2255. [CrossRef]

44. Jia, M.; Wang, Z.; Zhang, Y.; Mao, D.; Wang, C. Monitoring loss and recovery of mangrove forests during 42 years: The achievements of mangrove conservation in china. *Int. J. Appl. Earth Obs. Geoinf.* **2018**, *73*, 535–545. [CrossRef]
45. Schmitt, K.; Duke, N.C. Mangrove management, assessment and monitoring. In *Tropical Forestry Handbook*; Springer: Berlin/Heidelberg, Germany, 2015; pp. 1–29. [CrossRef]
46. Chen, L.; Wang, W.; Zhang, Y.; Lin, G. Recent progresses in mangrove conservation, restoration and research in china. *J. Plant Ecol.* **2009**, *2*, 45–54. [CrossRef]
47. Wang, Q.; Wang, H.; Zhang, W.; Wang, Z.; Xiao, D. The correlations between wetland landscape and social-natural factors on Northwestern Yunnan Plateau. *Acta Ecol. Sin.* **2019**, *39*, 726–738. Available online: https://kns.cnki.net/kcms/detail/11.2031.Q.20181018.1458.050.html (accessed on 1 September 2022). (In Chinese).